

# Experimental application of frequency-based approach to MIMO PI tuning via LMI constraints<sup>★</sup>

Anna Paula V de A Aguiar\* George Acioli Júnior\*  
Péricles R Barros\*

\* *Electrical Engineering Department - DEE  
Federal University of Campina Grande - UFCG  
PB, Brazil, (e-mail: anna.aguiar@ee.ufcg.edu.br,  
[georgeacioli,prbarros]@dee.ufcg.edu.br).*

---

**Abstract:** Multivariable (MIMO) processes are commonly found in the industry. The coupling between the different loops makes the controller design difficult. To solve the problem of controlling these processes, MIMO proportional integral (PI) controller design methods have been found in the literature. In this paper, the review and the experimental application of MIMO PI controller tuning methods with linear matrix inequalities constraints are presented. The considered tuning methods are formulated as a non-convex optimization problem. Linearization of the concave part around a known point is performed using the concave-convex procedure. Frequency-domain process data are used to solve problems. The application of the methods is done in two different processes: temperature module and Peltier module.

*Keywords:* PI controller; Controller design; Multivariable process; Convex optimization; Linear matrix inequalities.

---

## 1. INTRODUCTION

The proportional integral (PI) control is the most used controller in the industry (Nisi et al., 2019). This is a consequence of the simplicity of implementation and the good performance achieved in a variety of plants. The most common application of these controllers is in single input and single output (SISO) process and many of the design methods are based on the process model.

However, multivariable (MIMO) processes are often found in the industry. A characteristic of these processes is the coupling between the different loops. This coupling makes process model identification difficult and can degrade the control performance. Thus, the MIMO PI controller design is not simple.

The PI control structures for MIMO processes are classified as: decentralized control, centralized control and decoupled control. For strongly coupled processes, decentralized control may not result in the desired performance. So, the best performance of MIMO control loops is obtained with centralized control and decoupler control. Decoupler control can be treated as a particular case of centralized control.

The difficulty of modelling the MIMO process added to the development of technology and computer science resulted in the development of data-driven control design methods (DDC) (Luo et al., 2020). Although, the first DDC control design methods was proposed in 1993, many methods

have been proposed in the last twenty years (Formentin et al., 2019). In DDC methods it is not necessary to know the parametric process model. Time-domain or frequency-domain data can be used.

Designing MIMO PI controller that guarantee robustness and stability is not an easy task. Thus, optimization problems based on the 2-norm or  $\infty$ -norm and on frequency-domain data have been presented. In Galdos et al. (2010), a convex optimization problem is proposed to design the linearly parameterized centralized controller. To guarantee stability, the generalized Nyquist stability criterion is approximated by a set of convex constraints. The diagonal elements of the controller are tuned to satisfy the desired performance according to a reference model, while the remaining elements are designed to decouple the system.

In Hast et al. (2013), a convex optimization problem based on the  $\mathcal{H}_\infty$  norm and the frequency response of SISO processes is presented. The objective is to minimize the sensitivity function at low frequency. The extension of this method to stable MIMO processes is presented in Boyd et al. (2016), where to guarantee the closed-loop stability Linear Matrix Inequality (LMI) constraints are inserted into the problem. As the constraints are non-convex, the concave-convex procedure (Lipp and Boyd, 2016) is used. The result is a local optimum and depends on the algorithm initialization parameters.

Convex optimization and LMI constraints are also used in Karimi and Kammer (2017), where design methods based on  $\mathcal{H}_2$  and  $\mathcal{H}_\infty$  norms and loop shaping performance criteria are presented. In this case, the controller is fully parameterized in terms of matrix polynomial functions.

---

\* This work was supported by Conselho Nacional de Desenvolvimento Científico e Tecnológico (CNPq).

To make the initial problem convex, the concave-convex procedure is applied. The closed-loop stability is not guaranteed when the method based on loop shaping presented in Karimi and Kammer (2017) is used. Thus, control signal magnitude constraints are inserted into the optimization problem in Aguiar et al. (2021).

Practical aspects of the method that considers the  $\mathcal{H}_2$  norm are discussed in Kammer and Karimi (2018). Applications of these methods in the primary and secondary control of medium and low voltage networks, control of grid-connected inverters and control of energy converters of a particle accelerator are found in Kammer and Karimi (2019), Kammer et al. (2019) and Nicoletti et al. (2017), respectively.

In this paper, experimental results of PI MIMO control tuning methods formulated as a convex optimization problem with LMI constraints are presented. The methods proposed in Karimi and Kammer (2017) (loop shaping), Aguiar et al. (2021) and Boyd et al. (2016) are considered. The experiments are performed in a thermoelectric module. The centralized PI controller is considered.

This paper is organized as follows. The problem statement is presented in section 2. In the section 3, considered PI control design methods are revised. In section 4, implementation issues are commented. The module description used in the experiments and the experimental results discussion are presented in section 5. Finally, the conclusions are in section 6.

## 2. PROBLEM STATEMENT

Consider a MIMO stable process  $\mathbf{G}(s) \in \mathbb{C}^{n \times n}$ , where  $n$  is the number of inputs and outputs. The process parametric model is not known. The process frequency response ( $\mathbf{G}(j\omega)$ ),  $\forall \omega \in \mathbb{R}^+$ , is computed by the Fourier transform of the process input and output signals. Also consider a centralized controller  $\mathbf{C}(s) \in \mathbb{C}^{n \times n}$  given by:

$$\mathbf{C}(s) = \begin{bmatrix} C_{11}(s) & C_{12}(s) & \cdots & C_{1n}(s) \\ C_{21}(s) & C_{22}(s) & \cdots & C_{2n}(s) \\ \vdots & \vdots & \ddots & \vdots \\ C_{n1}(s) & C_{n2}(s) & \cdots & C_{nn}(s) \end{bmatrix}, \quad (1)$$

where each element  $C_{ij}(s)$  is a PI controller. Then:

$$\mathbf{C}(s) = \mathbf{K}_p + \frac{1}{s}\mathbf{K}_i \quad (2)$$

$\mathbf{K}_p$  and  $\mathbf{K}_i$  are proportional and integral gain matrices, respectively.

The loop gain function is given by:

$$\mathbf{L}(s) = \mathbf{G}(s)\mathbf{C}(s). \quad (3)$$

From the loop gain function the sensitivity functions are defined:

- closed-loop function or complementary sensitivity function:

$$\mathbf{T}(s) = \mathbf{L}(s)(\mathbf{I} + \mathbf{L}(s))^{-1}, \quad (4)$$

where  $\mathbf{I}$  is the identity matrix,

- sensitivity function:

$$\mathbf{S}(s) = (\mathbf{I} + \mathbf{L}(s))^{-1}, \quad (5)$$

- control sensitivity function:

$$\mathbf{Q}(s) = \mathbf{C}(s)(\mathbf{I} + \mathbf{L}(s))^{-1}. \quad (6)$$

The problem statement is: given the frequency response of the process, calculate the controller gain matrices ( $\mathbf{K}_p$  and  $\mathbf{K}_i$ ), without knowledge of the parametric process model.

## 3. MIMO PI CONTROL DESIGN

In this section, three multivariable PI controller tuning methods frequency-domain data-based are reviewed. The methods are formulated as a convex optimization problem. In two of them, LMI constraints are used to guarantee the stability of the designed closed-loop (sections 3.2 and 3.3). The methods presented in sections 3.1 and 3.2 are formulated considering a fully parameterized controller and rewritten for the PI controller. Frequency domain data can be obtained by Fourier transform of process input and output data or from a parametric model.

### 3.1 Loop shaping

The method presented in Karimi and Kammer (2017) goal to design a fully parametrized controller in terms of matrix polynomial functions. The control problem is formulated as optimization problem. The objective is to minimize the infinite norm of the difference between loop gain function ( $\mathbf{L}(s)$ ) and desired loop gain function ( $\mathbf{L}_d(s)$ ):

$$\min_{\theta} \|\mathbf{L}(s, \theta) - \mathbf{L}_d(s)\|_{\infty} \quad (7)$$

$\forall \omega > 0,$

where  $\theta$  is the parameters matrix. The problem (7) can be expressed as quadratic matrix inequality (QMI) form:

$$\begin{aligned} & \min_{\theta} \gamma \\ & \text{subject to:} \\ & (\mathbf{G}(s)\mathbf{C}(s, \theta) - \mathbf{L}_d(s))^* (\mathbf{G}(s)\mathbf{C}(s, \theta) - \mathbf{L}_d(s)) \leq \gamma \mathbf{I} \quad (8) \\ & \forall \omega > 0, \end{aligned}$$

where  $(\cdot)^*$  is a complex conjugate transpose and  $\gamma$  is a scalar variable

Consider  $\mathbf{C}(s, \theta) = \mathbf{X}(s, \theta)\mathbf{Y}^{-1}(s, \theta)$ . The convex optimization problem can be formulated from (8) using the Schur complement and concave-convex procedure (Lipp and Boyd, 2016). In this procedure the concave part is linearized around a known point  $\mathbf{C}_c(s) = \mathbf{X}_c(s)\mathbf{Y}_c^{-1}(s)$ . Thus, the controller is designed by solving the following convex optimization problem:

$$\begin{aligned} & \min_{\theta} \gamma \\ & \text{subject to:} \\ & \begin{bmatrix} \Psi(s, \theta) & (\mathbf{G}(s)\mathbf{X}(s, \theta) - \mathbf{L}_d(s)\mathbf{Y}(s, \theta))^* \\ (\mathbf{G}(s)\mathbf{X}(s, \theta) - \mathbf{L}_d(s)\mathbf{Y}(s, \theta)) & \gamma \mathbf{I} \end{bmatrix} \geq \mathbf{0} \\ & \forall \omega > 0, \end{aligned} \quad (9)$$

with  $\Psi(s, \theta) = \mathbf{Y}^*(s, \theta)\mathbf{Y}_c(s) + \mathbf{Y}_c^*(s)\mathbf{Y}(s, \theta) - \mathbf{Y}_c^*(s)\mathbf{Y}_c(s)$ .

When the PI controller is considered, the  $\mathbf{Y}(s)$  matrix is fixed. The convexification is not necessary. So, knowledge of an initialization controller is not required. For the PI controller, the problem (9) can be rewritten in the form:

$$\begin{aligned} & \min_{\theta} \gamma \\ & \text{subject to:} \\ & \begin{bmatrix} \mathbf{I} & (\mathbf{G}(s)\mathbf{C}(s, \theta) - \mathbf{L}_d(s))^* \\ (\mathbf{G}(s)\mathbf{C}(s, \theta) - \mathbf{L}_d(s)) & \gamma \mathbf{I} \end{bmatrix} \geq \mathbf{0} \quad (10) \\ & \forall \omega > 0. \end{aligned}$$

The algorithm converges to a local optimum or saddle point of the original non-convex problem. The designed controller not guarantee the closed-loop stability.

### 3.2 Loop shaping plus constraints

For stable processes, closed-loop stability can be ensured by limiting the a maximum value of the size of the closed-loop actuator signal (6) (Boyd et al., 2016), this is  $\|\mathbf{Q}(s, \theta)\|_\infty \leq Q_{max}$ . So, in Aguiar et al. (2021), the control signal magnitude bound is inserted as constraint into the optimization problem presented in Karimi and Kammer (2017).

The controller is designed by solving the optimization problem given by:

$$\begin{aligned} \min_{\theta} \quad & \|\mathbf{L}(s, \theta) - \mathbf{L}_d(s)\|_\infty \\ \text{subject to:} \quad & \\ & \|\mathbf{Q}(s, \theta)\|_\infty \leq Q_{max} \\ & \forall \omega > 0. \end{aligned} \quad (11)$$

The problem (11) can be rewritten in the QMI form:

$$\begin{aligned} \min_{\theta} \quad & \gamma \\ \text{subject to:} \quad & \\ & (\mathbf{G}(s)\mathbf{C}(s, \theta) - \mathbf{L}_d(s))^* (\mathbf{G}(s)\mathbf{C}(s, \theta) - \mathbf{L}_d(s)) \leq \gamma \mathbf{I} \\ & \mathbf{Q}^*(s, \theta)\mathbf{Q}(s, \theta) \leq Q_{max}^2 \mathbf{I} \\ & \forall \omega > 0. \end{aligned} \quad (12)$$

This problem is non-convex.

Consider the controller  $\mathbf{C}(s, \theta) = \mathbf{X}(s, \theta)\mathbf{Y}^{-1}(s, \theta)$  and the initialization controller  $\mathbf{C}_c(s) = \mathbf{X}_c(s)\mathbf{Y}_c^{-1}(s)$ . The convexification (Lipp and Boyd, 2016) is performed by linearizing the concave part around a known point ( $\mathbf{C}_c(s)$ ). Using the Schur complement, the constraints of (12) are written in the LMI form:

$$\begin{aligned} \min_{\theta} \quad & \gamma \\ \text{subject to:} \quad & \\ & \begin{bmatrix} \Psi(s, \theta) & (\mathbf{G}(s)\mathbf{X}(s, \theta) - \mathbf{L}_d(s)\mathbf{Y}(s, \theta))^* \\ \mathbf{G}(s)\mathbf{X}(s, \theta) - \mathbf{L}_d(s)\mathbf{Y}(s, \theta) & \gamma \mathbf{I} \end{bmatrix} \geq \mathbf{0} \\ & \begin{bmatrix} \mathbf{P}^*(s, \theta)\mathbf{P}_c(s) + \mathbf{P}_c^*(s)\mathbf{P}(s, \theta) - \mathbf{P}_c^*(s)\mathbf{P}_c(s) & \left(\frac{\mathbf{X}(s, \theta)}{Q_{max}}\right)^* \\ \frac{\mathbf{X}(s, \theta)}{Q_{max}} & \mathbf{I} \end{bmatrix} \geq \mathbf{0} \\ & \forall \omega > 0, \end{aligned} \quad (13)$$

with  $\mathbf{P}(s, \theta) = \mathbf{Y}(s, \theta) + \mathbf{G}(s)\mathbf{X}(s, \theta)$  and  $\mathbf{P}_c(s) = \mathbf{Y}_c(s) + \mathbf{G}(s)\mathbf{X}_c(s)$ .

For the PI controller, the convexification of the first constraint is not necessary. In this case, the problem (13) is rewritten in the form:

$$\begin{aligned} \min_{\theta} \quad & \gamma \\ \text{subject to:} \quad & \\ & \begin{bmatrix} \mathbf{I} & (\mathbf{G}(s)\mathbf{C}(s, \theta) - \mathbf{L}_d(s))^* \\ \mathbf{G}(s)\mathbf{C}(s, \theta) - \mathbf{L}_d(s) & \gamma \mathbf{I} \end{bmatrix} \geq \mathbf{0} \\ & \begin{bmatrix} \mathbf{P}^*(s, \theta)\mathbf{P}_c(s) + \mathbf{P}_c^*(s)\mathbf{P}(s, \theta) - \mathbf{P}_c^*(s)\mathbf{P}_c(s) & \left(\frac{\mathbf{C}(s, \theta)}{Q_{max}}\right)^* \\ \frac{\mathbf{C}(s, \theta)}{Q_{max}} & \mathbf{I} \end{bmatrix} \geq \mathbf{0} \\ & \forall \omega > 0, \end{aligned} \quad (14)$$

with  $\mathbf{P}(s, \theta) = \mathbf{I} + \mathbf{G}(s)\mathbf{C}(s, \theta)$  and  $\mathbf{P}_c(s) = \mathbf{I} + \mathbf{G}(s)\mathbf{C}_c(s)$ .

### 3.3 Low-frequency sensitivity

The method proposed by Boyd et al. (2016) aims to minimize the sensitivity function ( $\mathbf{S}(s)$ ) of the system for low frequency. For small values of  $s$ , we have that  $\mathbf{S}(s) \rightarrow (\mathbf{G}(0)\mathbf{K}_i)^{-1}$ . Therefore, the objective is given by:

$$\min \|\mathbf{G}(0)\mathbf{K}_i\|_\infty^{-1} \quad (15)$$

where  $\mathbf{G}(0)\mathbf{K}_i$  is non-singular matrix.

To guarantee stability and the lowest control effort, constraints that limit the maximum values of the sensitivity, complementary sensitivity and control sensitivity functions are added to the problem (15):

$$\begin{aligned} \min_{\theta} \quad & \|\mathbf{G}(0)\mathbf{K}_i\|_\infty^{-1} \\ \text{subject to:} \quad & \\ & \|\mathbf{S}(s, \theta)\|_\infty \leq S_{max} \\ & \|\mathbf{T}(s, \theta)\|_\infty \leq T_{max} \\ & \|\mathbf{Q}(s, \theta)\|_\infty \leq Q_{max} \\ & \forall \omega > 0. \end{aligned} \quad (16)$$

The optimization problem (16) can be written in the QMI form:

$$\begin{aligned} \min_{\theta} \quad & \gamma \\ \text{subject to:} \quad & \\ & ((\mathbf{G}(0)\mathbf{K}_i)^{-1})^* ((\mathbf{G}(0)\mathbf{K}_i)^{-1}) \leq \gamma \mathbf{I} \\ & (\mathbf{S}(s, \theta))^* (\mathbf{S}(s, \theta)) \leq S_{max}^2 \mathbf{I} \\ & (\mathbf{T}(s, \theta))^* (\mathbf{T}(s, \theta)) \leq T_{max}^2 \mathbf{I} \\ & (\mathbf{Q}(s, \theta))^* (\mathbf{Q}(s, \theta)) \leq Q_{max}^2 \mathbf{I} \\ & \forall \omega > 0. \end{aligned} \quad (17)$$

The convex optimization problem with LMI constraints is obtained from (17) using the Schur complement and convexifying the concave part, as done in the previous methods. Thus, the convex problem proposed by Boyd et al. (2016) is given by:

$$\begin{aligned} \min_{\theta} \quad & \gamma \\ \text{subject to:} \quad & \\ & \mathbf{Z}^*(s, \theta)\mathbf{Z}_c(s) + \mathbf{Z}_c^*(s)\mathbf{Z}(s, \theta) - \mathbf{Z}_c^*(s)\mathbf{Z}_c(s) - \gamma \mathbf{I} \geq \mathbf{0} \\ & \mathbf{P}^*(s, \theta)\mathbf{P}_c(s) + \mathbf{P}_c^*(s)\mathbf{P}(s, \theta) - \mathbf{P}_c^*(s)\mathbf{P}_c(s) - (\mathbf{I}/S_{max}^2) \geq \mathbf{0} \\ & \begin{bmatrix} \mathbf{P}^*(s, \theta)\mathbf{P}_c(s) + \mathbf{P}_c^*(s)\mathbf{P}(s, \theta) - \mathbf{P}_c^*(s)\mathbf{P}_c(s) & \left(\frac{\mathbf{L}(s, \theta)}{T_{max}}\right)^* \\ \frac{\mathbf{L}(s, \theta)}{T_{max}} & \mathbf{I} \end{bmatrix} \geq \mathbf{0} \\ & \begin{bmatrix} \mathbf{P}^*(s, \theta)\mathbf{P}_c(s) + \mathbf{P}_c^*(s)\mathbf{P}(s, \theta) - \mathbf{P}_c^*(s)\mathbf{P}_c(s) & \left(\frac{\mathbf{C}(s, \theta)}{Q_{max}}\right)^* \\ \frac{\mathbf{C}(s, \theta)}{Q_{max}} & \mathbf{I} \end{bmatrix} \geq \mathbf{0} \\ & \forall \omega > 0. \end{aligned} \quad (18)$$

where  $\mathbf{Z} = (\mathbf{G}(0)\mathbf{K}_i)^{-1}$ ,  $\mathbf{Z}_c = (\mathbf{G}(0)\mathbf{K}_{ic})^{-1}$ ,  $\mathbf{P}(s, \theta) = \mathbf{I} + \mathbf{G}(s)\mathbf{C}(s, \theta)$  and  $\mathbf{P}_c(s) = \mathbf{I} + \mathbf{G}(s)\mathbf{C}_c(s)$ .

## 4. EXPERIMENTAL RESULTS

In this section, two thermoelectric process are used to apply the multivariable PI controller design methods reviewed in this paper. Convex optimization problems are solved by Matlab's CVX framework (Grant and Boyd, 2008). The integral absolute error (IAE) and total value (TV) indices are used to compare controller performance.

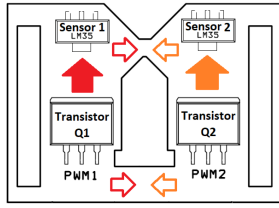


Figure 1. Schematics of the didactic module printed circuit board (Lima et al., 2018).

$$IAE = \int_0^{\infty} |\mathbf{r}(t) - \mathbf{y}(t)| dt \quad (19)$$

$$TV = \sum_{t=1}^{\infty} |\mathbf{u}(t+1) - \mathbf{u}(t)| \quad (20)$$

#### 4.1 Implementation issues

The formulated optimization problems are semi-infinite problems, because it have infinite constraints ( $\forall \omega > 0$ ). To enable the solution of the problems a finite and large set of frequencies was considered.

The frequency response of the process was obtained experimentally. The process was excited with a pseudo random binary signal (PRBS) signal. The PRBS signal clock period  $T_{ck}$  is defined as a function of the estimated dominant process time constant  $T_{st}$ :

$$T_{ck} = \frac{T_{st}}{5}. \quad (21)$$

Then, the Fourier transform of the collected input and output signals was performed.

The desired loop gain function ( $\mathbf{L}_d(s)$ ) was defined from the closed-loop function ( $\mathbf{T}_d(s)$ ). By definition:

$$\mathbf{T}(s) = \mathbf{L}(s)(\mathbf{I} + \mathbf{L}(s))^{-1}. \quad (22)$$

Considering a closed-loop reference model ( $\mathbf{T}_d(s)$ ), the desired loop gain function was given by:

$$\mathbf{L}_d(s) = \mathbf{T}_d(s)(\mathbf{I} - \mathbf{T}_d(s))^{-1}. \quad (23)$$

#### 4.2 Temperature module

The first process is the temperature model presented in Lima et al. (2018). The principle of this thermoelectric module is heat dissipation caused by field effect transistors semiconductors and heat propagation over a printed circuit board. The module consists of two transistors, two LM35 sensors, a printed circuit board and an Arduino board. Control is done by Matlab and communication by UBS. The schematics of the didactic module printed circuit is presented in Fig. 1, where the arrows indicate the expected spread of heat generated

The reference model and the initialization controller are given, respectively, by:

$$\mathbf{T}_d(s) = \begin{bmatrix} \frac{1}{47s+1}e^{-8.5s} & 0 \\ 0 & \frac{1}{19.56s+1}e^{-13s} \end{bmatrix} \quad (24)$$

and

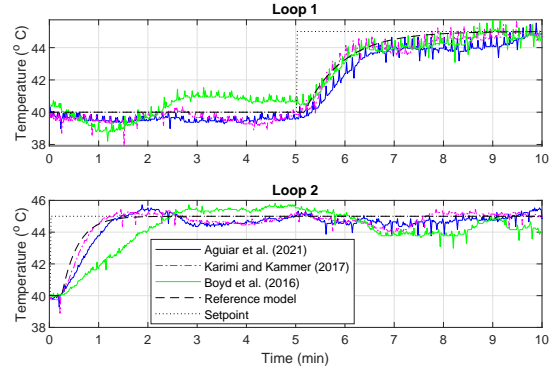


Figure 2. Closed-loop step response - Temperature module.

$$\mathbf{C}_i(s) = \begin{bmatrix} \frac{0.00015}{s} & \frac{-0.00009}{s} \\ \frac{-0.00009}{s} & \frac{0.00017}{s} \end{bmatrix}. \quad (25)$$

The other design parameters were  $Q_{max} = 0.0766$ ,  $T_{max} = 1.8$  and  $S_{max} = 1.8$ . The designed controllers gains are presented in Table 1.

Table 1. Controller gains - Temperature module.

	$C_{11}$		$C_{12}$	
	$K_p$	$K_i$	$K_p$	$K_i$
Aguiar et al. (2021)	0.028	0.0002	-0.010	-0.0003
Karimi and Kammer (2017)	0.042	0.0003	-0.012	-0.0004
Boyd et al. (2016)	0.029	0.0003	-0.019	-9 $10^{-5}$
	$C_{21}$		$C_{22}$	
	$K_p$	$K_i$	$K_p$	$K_i$
Aguiar et al. (2021)	-0.009	-0.0001	0.046	0.0004
Karimi and Kammer (2017)	-0.015	-0.0002	0.058	0.0005
Boyd et al. (2016)	-0.006	-0.0003	0.025	0.0003

The closed-loops step responses with the Aguiar et al. (2021), Karimi and Kammer (2017) and Boyd et al. (2016) controllers are presented in Fig. 2. Note that the closed-loops with the Aguiar et al. (2021) and Karimi and Kammer (2017) controllers approach the reference model. Being the lowest IAE achieved when the Karimi and Kammer (2017) controller is used, see Table 2.

The closed-loop with the Boyd et al. (2016) controller is smoother, observe the loop 2. In this case, the coupling between the loops is greater. This is a consequence of the smaller variation of the control signal, as seen in Fig. 3 and Table 2, where the control signal and the total variation are shown.

Table 2. Performance index - Temperature module.

	Loop 1	Loop 2
	Integral absolute error (IAE)	
Aguiar et al. (2021)	628.6	383.9
Karimi and Kammer (2017)	488.3	330.9
Boyd et al. (2016)	589.6	661.0
Total value (TV)		
Aguiar et al. (2021)	3.269	3.452
Karimi and Kammer (2017)	4.792	4.292
Boyd et al. (2016)	3.994	1.947

In this example, the smallest variation of the control signal was obtained with the Aguiar et al. (2021) controller, when

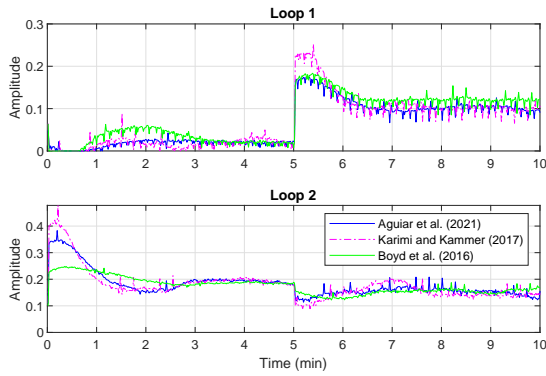


Figure 3. Input signal - Temperature module.

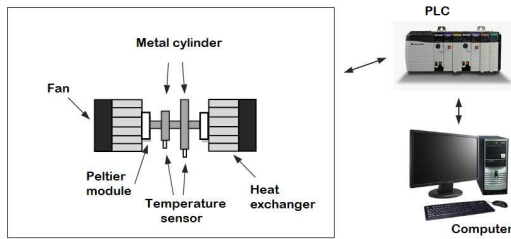


Figure 4. Peltier module diagram.

compared to the Karimi and Kammer (2017) controller. Furthermore, comparing Aguiar et al. (2021) and Boyd et al. (2016) controllers, note that for loop 2 there was a 41.93% reduction in the IAE when the Aguiar et al. (2021) controller was used. On the other hand, for loop 1 there was an increase of 6.5%.

#### 4.3 Peltier module

The Peltier module used is composed of two Peltier modules, two LM35 temperature sensors, two aluminium cylinders, two heat exchange and two fans. For temperature control, a programmable logic controller (PLC) - Rockwell Compact Logix L32E and a computer are used.

Each Peltier insert has a face attached to a heat exchange and a fan, to facilitate the exchange of heat with the environment, as shown in Fig. 4. The other side of the inserts is thermally coupled to a cylinder, in which the temperature sensors are fixed. Peltier modules are made up of thermoelectric chips, which operate as heat pumps. The temperature varies between 10°C and 70°C. Power is applied through PWM actuators.

The controller design is based on the open-loop frequency response. The reference model and the initialization controller, respectively, are given by:

$$\mathbf{T}_d(s) = \begin{bmatrix} \frac{1}{12s+1} e^{-2.74s} & 0 \\ 0 & \frac{1}{8s+1} e^{-2.52s} \end{bmatrix} \quad (26)$$

and

$$\mathbf{C}(s) = \begin{bmatrix} 1.125 + \frac{0.022}{s} & 0 \\ 0 & 1.049 + \frac{0.020}{s} \end{bmatrix}. \quad (27)$$

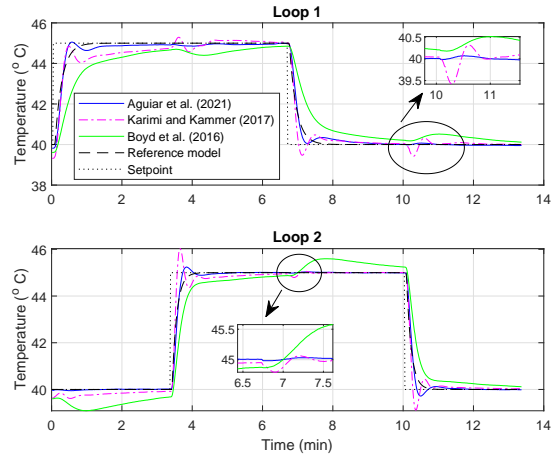


Figure 5. Closed-loop step response - Peltier module.

To design the controllers,  $Q_{max} = 110.94$ ,  $T_{max} = 1.8$  and  $S_{max} = 1.8$  were considered. The multivariable PI controllers designed with each method considered are presented in Table 3. Observe that the  $C_{12}$  and  $C_{21}$  parameters value are significantly lower than those of  $C_{11}$  and  $C_{22}$ . This is due to the weak coupling existing in this process.

Table 3. Controller gains - Peltier module.

	$C_{11}$		$C_{12}$	
	$K_p$	$K_i$	$K_p$	$K_i$
Aguiar et al. (2021)	2.677	0.041	-0.005	-0.005
Karimi and Kammer (2017)	4.885	0.045	1.070	-0.006
Boyd et al. (2016)	1.219	0.024	0.037	-0.012
	$C_{21}$		$C_{22}$	
	$K_p$	$K_i$	$K_p$	$K_i$
Aguiar et al. (2021)	0.016	-0.001	2.356	0.044
Karimi and Kammer (2017)	0.202	-0.002	4.635	0.044
Boyd et al. (2016)	0.014	-0.011	1.314	0.023

In Fig. 5, the closed-loops step responses with the Aguiar et al. (2021), Karimi and Kammer (2017) and Boyd et al. (2016) controllers are presented. Note that the closed-loop with the Aguiar et al. (2021) controller approaches the reference model. Furthermore, the Aguiar et al. (2021) loop showed lower coupling and IAE, see Table 4.

The controller of Karimi and Kammer (2017) is more aggressive, resulting in higher overshoot in loop 2, on the other hand, the response of loop 1 did not reach the reference when the step up was applied. The closed loop with the Boyd et al. (2016) controller is smoother and does not reach the steady state in the time period considered for each step, resulting in the highest IAE.

Table 4. Performance index - Peltier module.

	Loop 1	Loop 2
	Integral absolute error (IAE)	
Aguiar et al. (2021)	213.1	129.5
Karimi and Kammer (2017)	294.7	184.4
Boyd et al. (2016)	617.8	483.4
Total value (TV)		
Aguiar et al. (2021)	56.58	49.59
Karimi and Kammer (2017)	159.7	130.7
Boyd et al. (2016)	21.42	26.44

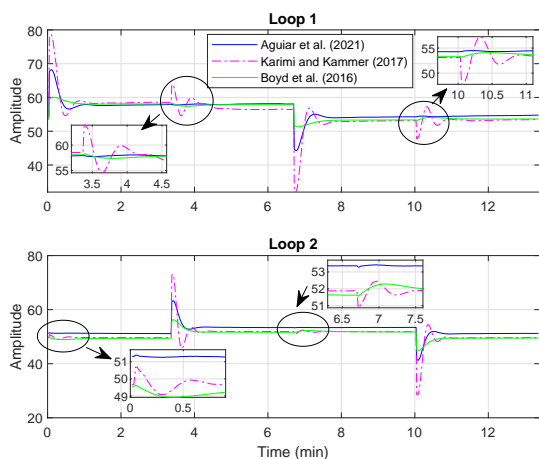


Figure 6. Input signal - Peltier module.

The control signals are shown in Fig. 6. The highest control signal was obtained with the Karimi and Kammer (2017) controller, as well as the highest control variation, as shown in Table 4. With the Aguiar et al. (2021) controller, lower control signal values were obtained when compared to Karimi and Kammer (2017), due to the constraints inserted in the optimization problem. However, the smoothest control signal and the smallest variation are obtained with the Boyd et al. (2016) controller.

In summary, with the Aguiar et al. (2021) controller, lower values of IAE and TV were obtained when compared to the controller of Karimi and Kammer (2017). In relation to the controller of Boyd et al. (2016), the TV of the Aguiar et al. (2021) controller was bigger, however the IAE reduced significantly. In this example, with the Aguiar et al. (2021) controller, it was possible to achieve the desired closed-loop response with the smallest possible control signal.

## 5. CONCLUSION

In this paper, experimental results from the application of PI MIMO controller design methods to a thermoelectric process were discussed. The considered methods are formulated as a convex optimization problem with LMI constraint. The open-loop process frequency response is used to solve the optimization problem.

All designed closed-loops were stable. The closed-loop response with the controller proposed by Karimi and Kammer (2017) was faster, with a more aggressive control signal. The controller signal proposed by Boyd et al. (2016) was smoother, with a very slow closed-loop response.

On the other hand, the controller proposed in Aguiar et al. (2021) presented at the same time the advantages of the controllers Karimi and Kammer (2017), response speed and Boyd et al. (2016), smoothness of the control signal. Thus, for the thermoelectric processes studied, the method presented in Aguiar et al. (2021) resulted in the best performance when compared to the other methods considered.

## REFERENCES

Aguiar, A.P.V.d.A., Acioli Júnior, G., Barros, P.R., and Perkusich, A. (2021). A data-driven approach to MIMO

PID tuning via LMI constraints. In *2021 Modeling, Estimation and Control Conference (MECC)*, volume 54, 573–578. IFAC, EUA.

Boyd, S., Hast, M., and Åström, K.J. (2016). MIMO PID tuning via iterated LMI restriction. *International Journal of Robust and Nonlinear Control*, 26(8), 1718–1731.

Formentin, S., Campi, M.C., Carè, A., and Savaresi, S.M. (2019). Deterministic continuous-time virtual reference feedback tuning (VRFT) with application to pid design. *Systems & Control Letters*, 127, 25–34.

Galdos, G., Karimi, A., and Longchamp, R. (2010).  $H_\infty$  controller design for spectral MIMO models by convex optimization. *Journal of Process Control*, 20(10), 1175–1182.

Grant, M.C. and Boyd, S.P. (2008). Graph implementations for nonsmooth convex programs. In *Recent Advances in Learning and Control. Lecture Notes in Control and Information Sciences*, volume 371, 95–110. Springer, Inglaterra.

Hast, M., Åström, K., Bernhardsson, B., and Boyd, S. (2013). PID design by convex-concave optimization. In *2013 European Control Conference (ECC)*, 4460–4465. IEEE, Suíça.

Kammer, C., D’Arco, S., Endegnanew, A.G., and Karimi, A. (2019). Convex optimization-based control design for parallel grid-connected inverters. *IEEE Transactions on Power Electronics*, 34(7), 6048–6061.

Kammer, C. and Karimi, A. (2018). A data-driven fixed-structure control design method with application to a 2-DOF gyroscope. *2018 IEEE Conference on Control Technology and Applications (CCTA)*, 915–920.

Kammer, C. and Karimi, A. (2019). Decentralized and distributed transient control for microgrids. *IEEE Transactions on Control Systems Technology*, 27(1), 311–322.

Karimi, A. and Kammer, C. (2017). A data-driven approach to robust control of multivariable systems by convex optimization. *Automatica*, 85, 227–233.

Lima, A.B., Barros, P.R., and Acioli Júnior, G. (2018). Módulo didático para ensino de teoria de controle. In *XXII Congresso Brasileiro de Automática (CBA)*. doi: <http://dx.doi.org/10.20906/cps/cba2018-1043>.

Lipp, T. and Boyd, S. (2016). Variations and extension of the convex-concave procedure. *Optimization and Engineering*, 17(2), 263–287.

Luo, H., Yin, S., Liu, T., and Khan, A.Q. (2020). A data-driven realization of the control-performance-oriented process monitoring system. *IEEE Transactions on Industrial Electronics*, 67(1), 521–530.

Nicoletti, A., Martino, M., and Karimi, A. (2017). A data-driven approach to power converter control via convex optimization. *2017 IEEE Conference on Control Technology and Applications (CCTA)*, 1466–1471.

Nisi, K., Nagaraj, B., and Agalya, A. (2019). Tuning of a PID controller using evolutionary multi objective optimization methodologies and application to the pulp and paper industry. *International Journal of Machine Learning and Cybernetics*, 10(8), 2015–2025.